International Journal for Housing Science and Its Applications

Publish September 24, 2025. Volume 47, Issue 1 Pages 1180–1190

https://doi.org/10.70517/ijhsa471102

Improved YOLOv8-CDSL Network for Detecting Defects of the Printed Circuit Board

Dapeng Feng[1,2], Mengmeng Zhang[1,2], Zhao Zhang[1,*] and Shaoan Tian[3]

[1] School of Mechanical and Electronic Engineering, Hubei Polytechnic University, Huangshi, 435003, China

[2] Hubei Key Laboratory of intelligent transportation technology and device, Hubei Polytechnic University, Huangshi, 435003, China

[3] Hubei Zhongpei Electronics Technology Co., Ltd, Huangshi, 435200, China

Corresponding authors: (e-mail: fdp201015@sina.com).

Abstract Aiming at the problem of high false detection rate of PCB defect detection,an improved YOLOv8-C2f_DBB-SPFF_LSKA (YOLOv8-CDSL) is used to detect defects of the PCB. The diverse branch block (DBB) is used to improve the faster version of CSP bottle-neck with two convolutions (C2f) module in the YOLOv8 backbone network. The large separable kernel attention (LSKA) mechanism is also added to the SPPF module of the YOLOv8 network. The C2F_DBB module can significantly improve the model's ability to identify small-scale PCB defects, and greatly enhance the model's performance in comprehensive feature extraction. Thus significantly improving the overall accuracy of the model. The SPPF_LSKA module can reduce the computing power consumption of model training. Consequently, it significantly enhances the detection capability of the improved YOLOv8-CDSL network. The effectiveness of the improved scheme was verified by ablation experiments. At the same time, it is verified by comparative experiments that the improved YOLOv8-CDSL network has the highest detection accuracy of 99.13% for six common surface defects of PCB.

Index Terms YOLOv8, C2f_DBB, SPPF_LSKA, Defect detection, Printed circuit board

I. Introduction

With the rapid advancement of China's modern electronics industry and emerging technologies, printed circuit board (PCB) serves as the essential hardware support for wiring connection and signal transmission in various electronic products as the carrier of diverse electronic components [1]. The intricate production process and complex manufacturing environment of PCB can easily lead to various imperfections during manufacturing [2], which in turn can impact the performance of the PCB. High quality detection of PCB surface defects is a crucial task in the manufacturing process.

At present, the common defects detection methods for printed circuit boards include functional testing [3], online testing [4], manual eye inspection [5], and visual inspection technology [6]. In the application of online testing and functional testing, it is necessary to design complex test circuits and test schemes, and the test circuits and schemes of different PCB products are also different [7]. Some defects are undetectable. The traditional manual eye inspection method has some problems, such as low efficiency, high cost, low accuracy, and strong subjective factors [8]. Which is gradually replaced by machine vision technology [9]. Machine vision inspection technology relies on artificial intelligence algorithms and utilizes image processing and pattern recognition to achieve rapid automatic identification of PCB defects. It is characterized by its cost-effectiveness, high efficiency, and strong robustness [10]. Wu et al. [11] developed an automatic PCB visual inspection system based on pixel processing, which directly subtracts template images from the detected image to locate defects in the PCB, thus greatly reducing the inspection processing time. Liu et al. [12] proposed a key technology for PCB defect online detection based on machine vision to detect, locate, and identify simple geometric defects such as short circuit, open circuit, and burr that may occur on PCB production lines. Although there are many PCB defect detection methods, each method has inherent limitations and shortcomings, and the selection of detection methods must be consistent with the specific requirements and situations.

Several studies [13], [14] have implemented various deep learning models to detect PCB surface defects. Zhang et al. [15] proposed a method for PCB defect detection based on a convolution neural network (CNN) model. They utilized a deep pre-trained convolutional neural network to extract discriminant features of defects, which demonstrated sufficient ability to distinguish between different types of defects. Ding et al. [16] proposed a neural network for the detection of micro-defects in PCBs, leveraging the inherent multi-scale and pyramid hierarchy structure of deep convolutional networks to construct feature pyramids. The robustness of the neural network was validated through ablation experiments, achieving a mean average precision (mAP) of 98.90%. Shen et al. [17] established a new lightweight CNN model for PCB component inspection. The detection accuracy of 12 different electronic components is improved to 85.8%.

YOLO (You only look once, YOLO) series network is a typical single-stage target detection method, it has been widely used in the field of defect detection in recent years [18]. Mamidi et al. [19] introduced a lightweight YOLOv4-tiny network for the identification and classification of defects in printed circuit boards. The attained mAP of 79.72% across six distinct defect types showcases its effectiveness in this field, demonstrating impressive results. Wang et al. [20] proposed a lightweight underwater object detection model based on YOLOv6. a lighter backbone network was developed by incorporating the ODConv module into the rebuilt EfficientNetv2, aiming to reduce the number of parameters and floating point operations. Li et al. [21] proposed a lightweight aluminum surface defect detection model, M2-BL-YOLOv4, which was based on the YOLOv4 algorithm. The complex CSPDark-Net53 backbone network was restructured into an inverted residual structure, leading to a significant reduction in model parameters and an improved detection speed. The findings indicated that the enhanced M2-BL-YOLOv4 achieves an average accuracy of 93.5%. The lightweight network was capable of effectively fulfilling its tasks, although extensive training with a large dataset was necessary to obtain a stable model. Ling et al. [22] proposed a novel CNN model for dense PCB component detection by incorporating several modifications into YOLOv8. The proposed model achieved the highest mean average precisions of 87.7% (mAP@0.5) and 75.3% (mAP@0.5:0.95) respectively, surpassing other state-of-the-art models. However, the performance of this method in unbalanced PCB defect samples needed to be further improved. Xia et al. [23] designed a global contextual attention augmented YOLO model with ConvMixer prediction heads (GCC-YOLO) to solve the problem of missed and false detection caused by the large number of tiny targets and complex background textures in PCB. The GCC-YOLO improved the precision, recall, mAP@0.5, and mAP@0.5:0.95 by 0.2%, 1.8%, 0.5%, and 8.3%, respectively, compared to YOLOv5s. Moreover, it had a smaller model volume and faster reasoning speed compared to other algorithms. But the detection precision for the relatively large-sized spurious copper type defect had a lower precision value by the GCC-YOLO.

However, the detection accuracy and speed of existing models need further improvement in order to achieve batch and accurate detection of PCB, given their large size difference, diverse appearance, and dense distribution.

The YOLO framework exhibits superior performance in the detection of minute defects [24]. In this study, an improved YOLOv8-C2f_DBB-SPFF_LSKA (YOLOv8-CDSL) is used to detect defects of the PCB. The diverse branch block (DBB) is used to improve the faster version of CSP bottleneck with two convolutions (C2f) module in the YOLOv8 backbone network. The large separable kernel attention (LSKA) mechanism is also added to the SPPF module of the YOLOv8 network. The C2F_DBB module can significantly improve the model's ability to identify small-scale PCB defects, and greatly enhance the model's performance in comprehensive feature extraction. Thus significantly improving the overall accuracy of the model. The SPPF_LSKA module can reduce the computing power consumption of model training. Consequently, it significantly enhances the detection capability of the improved YOLOv8-CDSL network.

II. MATERIAL AND METHODS

II. A. Typical surface defects of PCB

PCB has evolved from single-layer to double-sided, multi-layer, and flexible configurations while maintaining its own developmental trajectory. As it continues to advance towards higher precision, density, and reliability, PCBs are becoming smaller in size, more cost-effective, and increasingly high-performing. The manufacturing process of the PCB is shown in Figure 1.

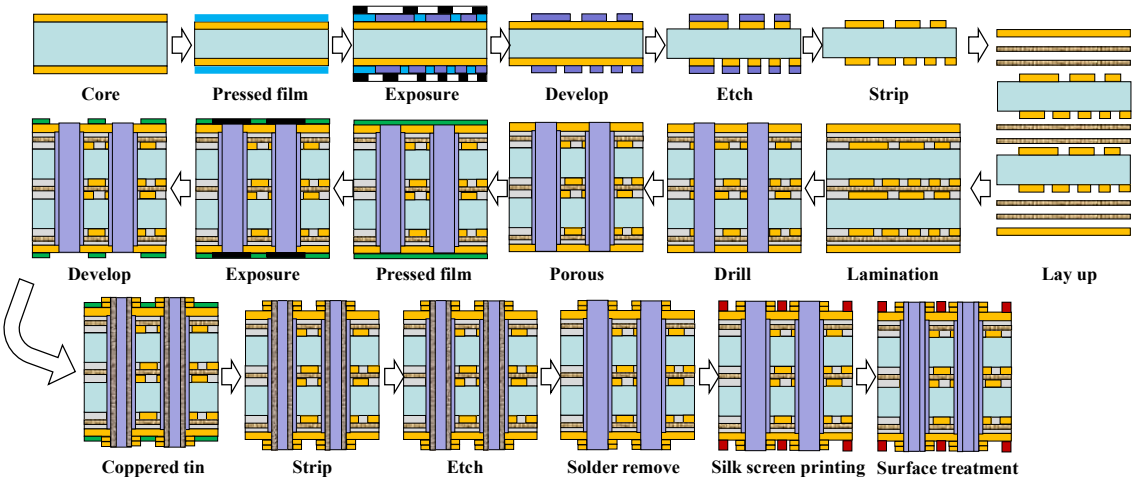

Figure 1: Manufacturing process of the PCB.

The manufacturing process of the mainly includes pressed film, exposure, develop, etch, strip, testing, and other key processes. The manufacturing processes of PCB are varied and the processing environments are complex. It is easy to cause a variety of defects. The typical surface defects of PCB include missing hole, mouse bite, short, spur, open circuit, and spurious copper [25]. The typical surface defects of PCB are shown in Figure 2. The identification of PCB surface defects has become a critical process in ensuring the quality of PCB production, as these flaws not only significantly impact the final product's performance and quality, but also result in substantial economic losses for related industries. This has garnered significant attention from the industry.

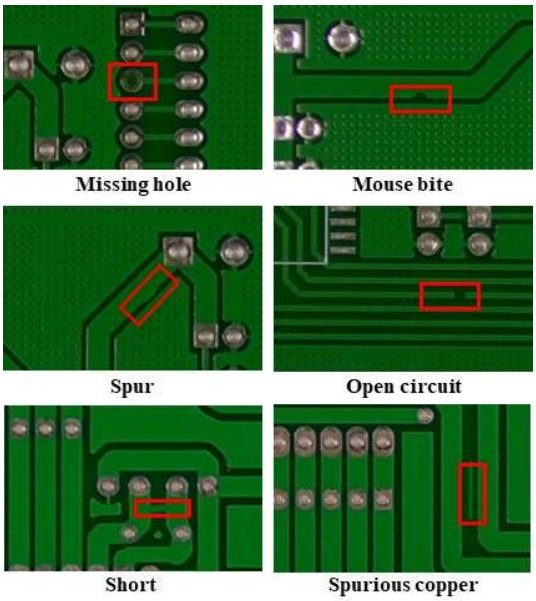

Figure 2: Typical surface defects of PCB.

II. B. Structure of the improved YOLOv8-CDSL network

The you only look once (YOLO) series model is an effective single-stage target detection algorithm within the field of target detection [26]. YOLOv8 model has been widely used in the field of small size defect detection in recent years [27]. With the continuous iteration of YOLO, the network performance of the network has become more and more powerful. YOLOv8 is a state-of-the-art (SOTA) model incorporating a novel backbone network, anchor-less detector, and loss function [28]. The YOLOv8 network incorporates an attention mechanism and optimization strategy to enhance the accuracy and performance of target detection. The YOLOv8 framework is comprised of five distinct sizes: nano, small, medium, large, and xtra-large [29]. Based on YOLOv8-nano network, an improved YOLOv8-C2f_DBB-SPFF-LSKA (YOLOv8-CDSL) network is proposed. The structure of the improved YOLOv8- CDSL network for defect detection of the PCB is shown in Figure 3. Based on the YOLOv8-nano backbone network, the improved YOLOv8-CDSL network used a diverse branch block (DBB) to replace a Bottleneck convolution in the existing C2f module. The replacement module is denoted as C2f_DBB. Replace the C2f modules of layers 3, 5, 7, and 9 in the YOLOv8-nano network with C2F_DBB modules. Another improvement is the addition of large separable kernel attention (LSKA) in the SPPF module. This enhancement can expand the acceptance range of the convolutional structure while consuming less computational power, and thoroughly explore the internal connections within PCB defect image information.

In the basic YOLOv8 network architecture, the bottleneck module of C2f is usually used to perform dimensionality reduction tasks in feature dimensions. However, convolution operations inside the module may result in partial loss of spatial information, thus limiting the model's ability to fully express features. Especially when dealing with PCB defect data sets, due to the diversity of defect scales, the performance of the original bottleneck module in extracting multi-scale defect features is not ideal, resulting in lower detection accuracy and lower processing efficiency. The structure of the C2f_DBB module in the improved YOLOv8-CDSL network is shown in Figure 4.

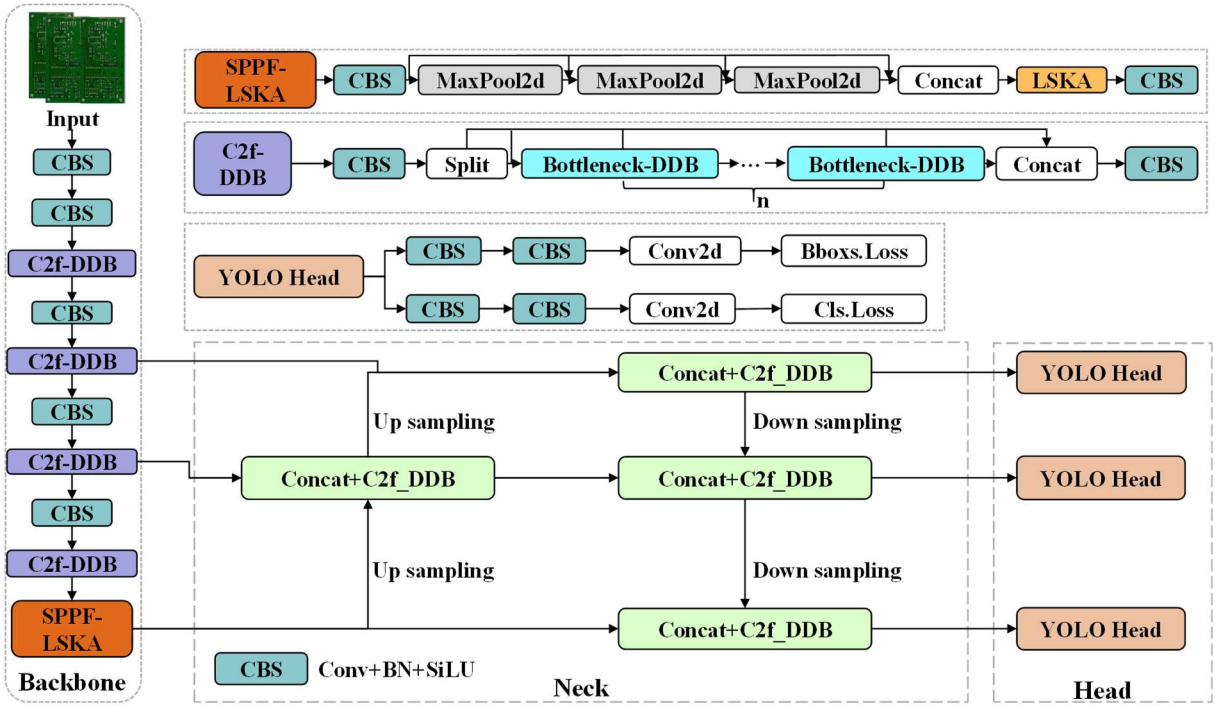

Figure 3: Improved YOLOv8-CDSL network structure for defect detection of the PCB.

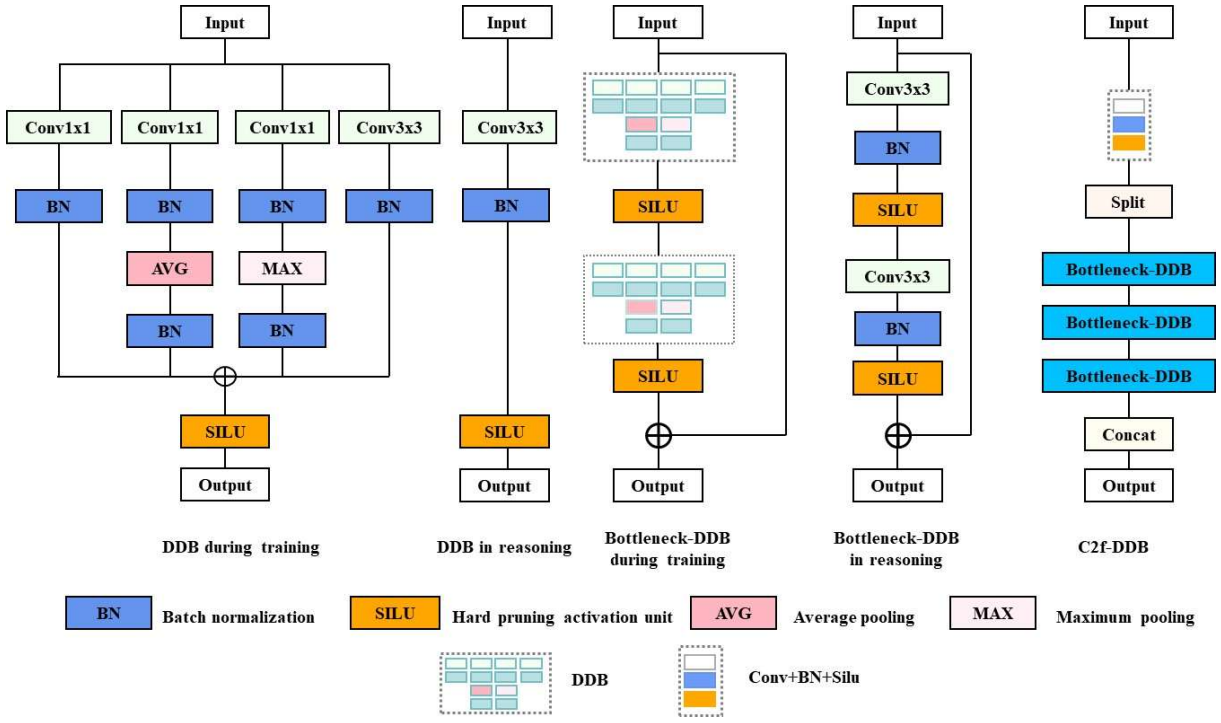

Figure 4: Structure of the C2f_DBB module in the improved YOLOv8-CDSL network.

The convolutional structure within the C2f_DBB module encompasses a series of branches involving convolution, multi-scale convolution, and average pooling operations. These intricate branches are simplified back to simple convolutions during inference. This paper introduces the addition of 4 branch-specific convolution operations by channels, with the first branch consisting of 1×1 convolution followed by batch normalization. The second branch involves 1×1 convolution and batch normalization followed by average pooling and additional batch normalization. The third branch includes 1×1 convolution and batch normalization followed by maximum pooling and another round of batch normalization using 1×1 convolutions. Lastly, the fourth branch consists of a 3×3 convolution followed by batch normalization. These four branches then combine channels

before passing through a non-linear layer, constituting the DBB module utilized in this study. The multi-branch topology of DBB, combined with paths of varying scales and complexity, serves to enrich the feature space and enhance model detection performance. The DBB module introduces complexity during training, but reverts to the original inference structure during actual inference, thereby decoupling the network structure between training and inference times. In this study, the DBB module replaces Conv in the Bottleneck module of C2f, resulting in improved performance of the YOLOv8 network with the introduction of the C2F_DBB module.

The LSKA module is utilized to enhance the SPPF module in the original YOLOv8, resulting in a larger receptive field while conserving memory and computational resources. LSKA functions as an attention mechanism by stacking large kernels and connecting cascade depth-wise convolution (DW-Conv) and dilated depth-wise convolution (DW-D-Conv) to capture local intrinsic dependencies of images. The structure of the SPPF-LSKA module in the improved YOLOv8-CDSL network is shown in Figure 5.

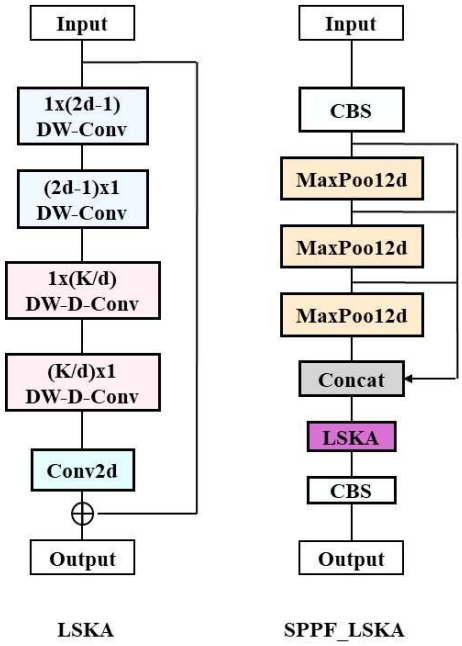

Figure 5: Structure of the SPPF_LSKA module in the improved YOLOv8-CDSL network.

The SPPF_LSKA module is implemented by adding LSKA to the existing structure of SPPF. Compared with ordinary $K\times K$ convolution, LSKA disassembles it into four convolutions of $1\times(2d-1)$, $(2d-1)\times 1$, $1\times(K/d)$, and $(K/d)\times 1$. The optimization strategy is to first replace $K\times K$ ordinary convolution with a cascade deep convolution of $(2d-1)\times(2d-1)$ and $(K/d)\times(K/d)$ extended deep convolution to introduce a larger convolution kernel, and further separate the convolution kernel of $(2d-1)\times(2d-1)$ into a convolution kernel of $1\times(2d-1)$ and $(2d-1)\times 1$. The $(K/d)\times(K/d)$ convolution kernel is separated into $1\times(K/d)$ and $(K/d)\times 1$ convolution kernels, and the second increase in the number of parameters caused by larger convolution kernels is suppressed by this separation. Moreover, it effectively suppresses the secondary increase in parameter count when increasing kernel size.

II. C. Loss function of the improved YOLOv8-CDSL network

The regression loss for the object detection bounding box in YOLOv8 consists of two components. The first component is the distributed focus loss (DFL), which utilizes cross-entropy as an optimization mechanism to align the predicted distribution of the network with the label value. The second component involves using the complete intersection over union (CIoU) loss measure to compute the cross-linking (IoU) between the prediction and true bounding box [30]. The final regression loss is a weighted sum of these two parts, utilizing specific weight coefficients. The CIoU loss is calculated as follows [27]:

$$L_{CIoU}=1-IoU+\frac{\rho^2(b,b_{gt})}{(w_c)^2+(h_c)^2}+\alpha v \tag{1}$$

where

$$\alpha = \frac{\nu}{(1 - IoU) + \nu} \tag{2}$$

$$\nu = \frac{4}{\pi^2}(\arctan\frac{w_{gt}}{h_{gt}} - \arctan\frac{w}{h})^2 \tag{3}$$

where w_c and h_c represent the width and height of the minimum bounding rectangle of the prediction box and the target box, while w and h denote the width and height of the prediction box. Similarly, w_{gt} and h_{gt} indicate the width and height of the target box respectively. Additionally, b and b_{gt} are used to denote the boundary center points of the prediction box and the target box respectively. ρ represents the Euclidean distance between b and b_{gt}.

The DFL optimizes the probability of the two nearest locations to the label using cross-entropy, allowing the network to quickly focus on the local distribution of the target location. The weight of its neighboring integer coordinates is determined through linear interpolation. The DFL is calculated as follows:

$$DFL(S_i, S_{i+1}) = -((y_{i+1} - y)\log(S_i) + (y - y_i)\log(S_{i+1})) \tag{4}$$

where

$$S_i = \frac{y_{i+1} - y}{y_{i+1} - y_i} \tag{5}$$

$$S_{i+1} = \frac{y - y_i}{y_{i+1} - y_i} \tag{6}$$

where y represents the general distribution value, i denotes the label number. S_i indicates the probability of the predicted value y_i being close to the label.

III. RESULTS

III. A. Datasets of the improved YOLOv8-CDSL network

In order to verify the effectiveness and superiority of the improved YOLOv8-CDSL network, a large number of sample data detection is required. Hence, according to the PCB defect dataset released by Peking University, there are a total of 693 images in PKU-Market-PCB [31]. The dataset contains six typical surface defects missing hole, mouse bite, short, spur, open circuit, and spurious copper. The study in this paper utilizes exclusively the images from this publicly available dataset and reclassifies the defects.

Due to the limited number of samples in the PKU-Market-PCB and the small ratio of defect target size to sample size, direct use of the data for training may lead to overfitting and poor training results. To address these issues, the mosaic random data augmentation technology is employed to process sample data and enhance the diversity of defect targets [32]. Thereby improving the training characteristics of the YOLOv8-CDSL network. The hyperparameters associated with the mosaic random data augmentation is shown in Table 1.

Table 1: Hyperparameters associated with the mosaic random data augmentation.

Parameters	Parameters definitions	Value
HSV-hue	Randomly adjust the hue of images	0.03
HSV-saturation	Randomly adjust the saturation of images	0.95
HSV-value	Randomly adjust the value of images	0.5
Image scale	Scale images	0.6
Rotate	Randomly rotate images	15
Flip	Randomly flip images horizontally	10
Mosaic	Randomly spliced mixed images	1

Through random data enhancement technique, the data set is expanded effectively. The total of images is 6930. The size of the defect sample data is 640*640 pixels. The dataset is partitioned into training, validation, and test sets in an 8:1:1 ratio. The dataset division of PCB defect images in training, verification, and test datasets is shown in Figure 6.

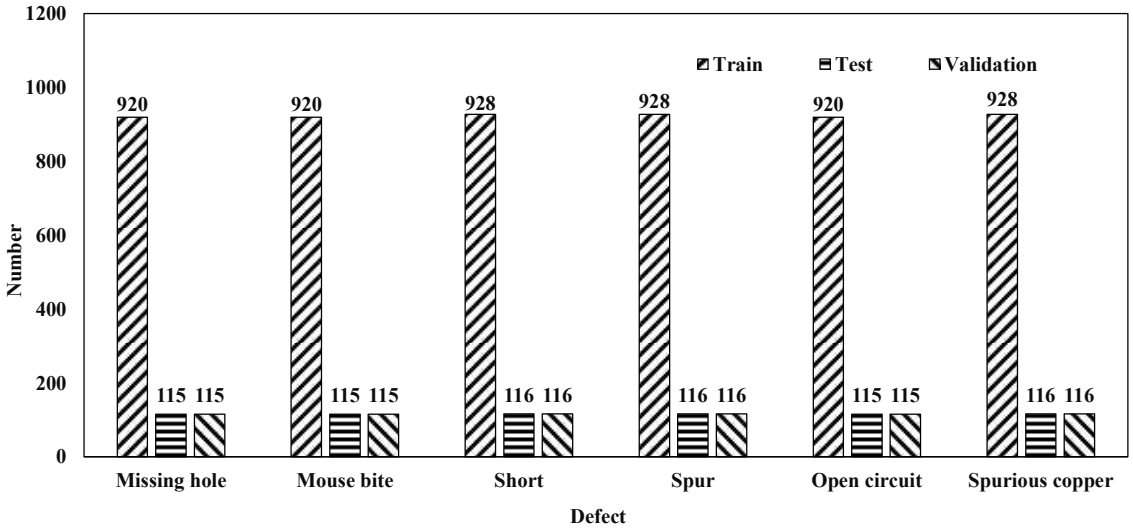

Figure 6: Dataset division of PCB defect images in training, verification, and test datasets.

III. B. Ablation experiments of the improved YOLOv8-CDSL network

To assess the efficacy of the improved YOLOv8-CDSL network, derived from the YOLOV8-nano network, successive ablation experiments are conducted by incrementally incorporating the improved modules.

During the training process, the average precision (*AP*) is utilized for evaluating the test results, as it provides a balanced assessment of both precision (*P*) and recall (*R*) [33]. The normal sample is classified as positive (*P*), while the defective sample is classified as negative (*N*). The trained model makes predictions on the polarity of the input sample, categorizing it as either positive or negative. Positive samples are labeled as true (*T*), and negative samples are labeled as false (*F*) [34]. The predicted results can be described in terms of true positive (*TP*), true negative (*TN*), false positive (*FP*), and false negative (*FN*). The *P* and *R* are calculated as follows:

$$precision = \frac{TP}{TP + FP} \tag{7}$$

$$recall = \frac{TP}{TP + FN} \tag{8}$$

The *AP* and *mAP* are calculated as the follow

$$AP = \int_0^1 P(r)dr \tag{9}$$

$$mAP = \frac{\sum AP}{k} \tag{10}$$

where *P(r)* is the *P*–*R* curve plotted by precision and recall values. The AP metric offers a comprehensive evaluation of accuracy and recall by taking into account the area under the *P*-*R* curve [35]. *T* is the number of the PCB surface defect classes.

The algorithm described in this paper is implemented using PyCharm Community Edition 2024.1.4 software (JetBrains, Czech Republic). The hardware setup for all experiments consisted of an Intel(R) Xeon(R) E5-2680 @ 2.70 GHz (16 GB RAM) CPU and NVIDIA Quadro RTX 3060 GPU. Additionally, all neural networks were trained using the adam optimizer with a fixed learning rate of 0.0001.

The YOLOv8-nano network, which includes C2f and SPFF modules, served as the basis for the ablation experiment. Subsequently, the DBB module and LSKA module are added to the C2f and SPFF modules for comparison, resulting in YOLOv8-C2f_DBB and YOLOv8-SPFF_LSKA network. These were then compared with the improve YOLOv8-CDSL network. The epoch set as 100. Figure. 7 shows the training loss and validation loss of the network in detecting defects of the PCB. It can be seen from the data the improved YOLOv8-CDSL network has the lowest training loss and good training characteristics.

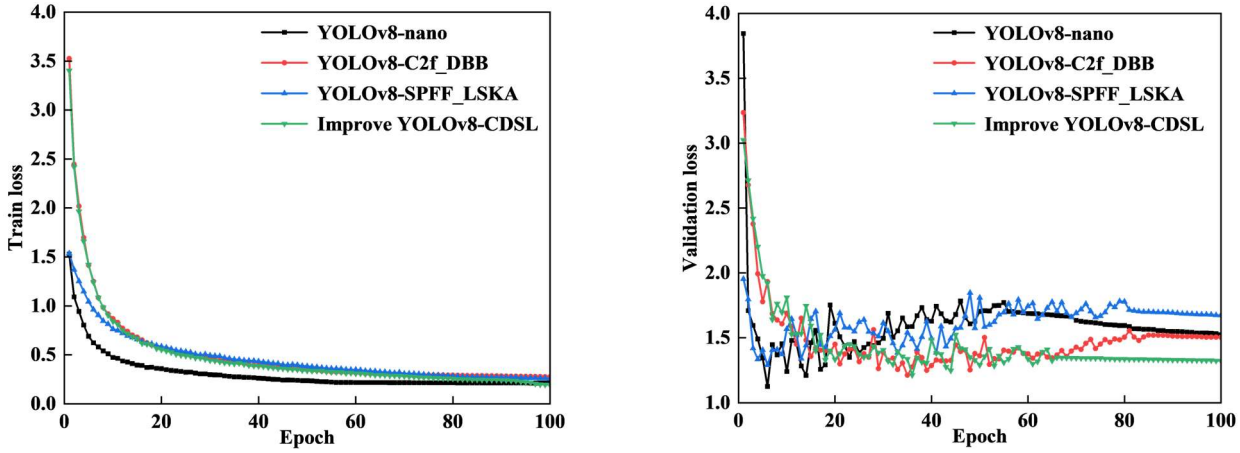

Figure 7: Training loss and validation loss of the network in detecting defects of the PCB.

The results of the ablation experiments of the networks are shown in Table 2. By incorporating the DBB module and LSKA module into the YOLOv8-nano network, the detection performance for PCB defects can be significantly improved. The *P* of the improved YOLOV8-CDSL network is 5.58%, 3.69%, and 2.85% higher than that of YOLOv8-nano, YOLOv8-C2f_DBB, and YOLOv8-SPFF_LSKA networks respectively. The *R* of the improved YOLOV8-CDSL network is 6.97%, 3.67%, and 1.07% higher than that of YOLOv8-nano, YOLOv8-C2f_DBB, and YOLOv8-SPFF_LSKA networks respectively. The *mAP* of the improved YOLOV8-CDSL network is 2.73%, 1.87%, and 0.98% higher than that of YOLOv8-nano, YOLOv8-C2f_DBB, and YOLOv8-SPFF_LSKA networks respectively.

Table 2: Results of the ablation experiments of the networks.

Network	*P*	*R*	*mAP*
YOLOv8-nano	93.57%	91.47%	97.24%
YOLOv8-C2f_DBB	95.27%	94.39%	98.06%
YOLOv8-SPFF_LSKA	96.05%	96.81%	98.92%
Improved YOLOv8-CDSL	98.79%	97.85%	99.89%

III. C. Defect detection results of the PCB

Comparative experiments were conducted to validate the superiority of the improved YOLOv8-CDSL network for PCB surface defect detection, using YOLOv8-nano [36], YOLOv5 [37], and YOLOv6 [38] networks as comparators under identical dataset and parameter conditions. The epoch set as 100. The comparison of the accuracy of the networks in detecting defects of the PCB is shown in Figure. 8. These networks are capable of effectively detecting surface defects on PCBs. Notably, the improved YOLOv8-CDSL network demonstrated faster and more significant improvements in training and validation accuracy, allowing the prediction box to closely approach ground truth values. The inflection point of the improved YOLOv8-CDSL network occurs earlier than that of YOLOv8-nano, YOLOv5, and YOLOv6 networks. The results indicate that the improved YOLOv8-CDSL network exhibits a faster and more stable convergence speed.

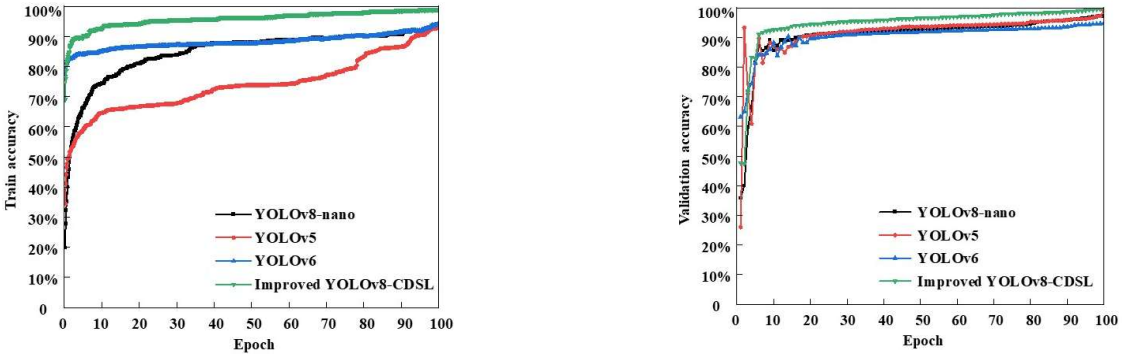

Figure 8: Comparison of the accuracy of the networks in detecting defects of the PCB.

The four comparison networks demonstrate high accuracy in detecting the six common defects of PCB, as shown in Figure 9. The numbers are the probability of these networks detecting the different PCB surface defects.

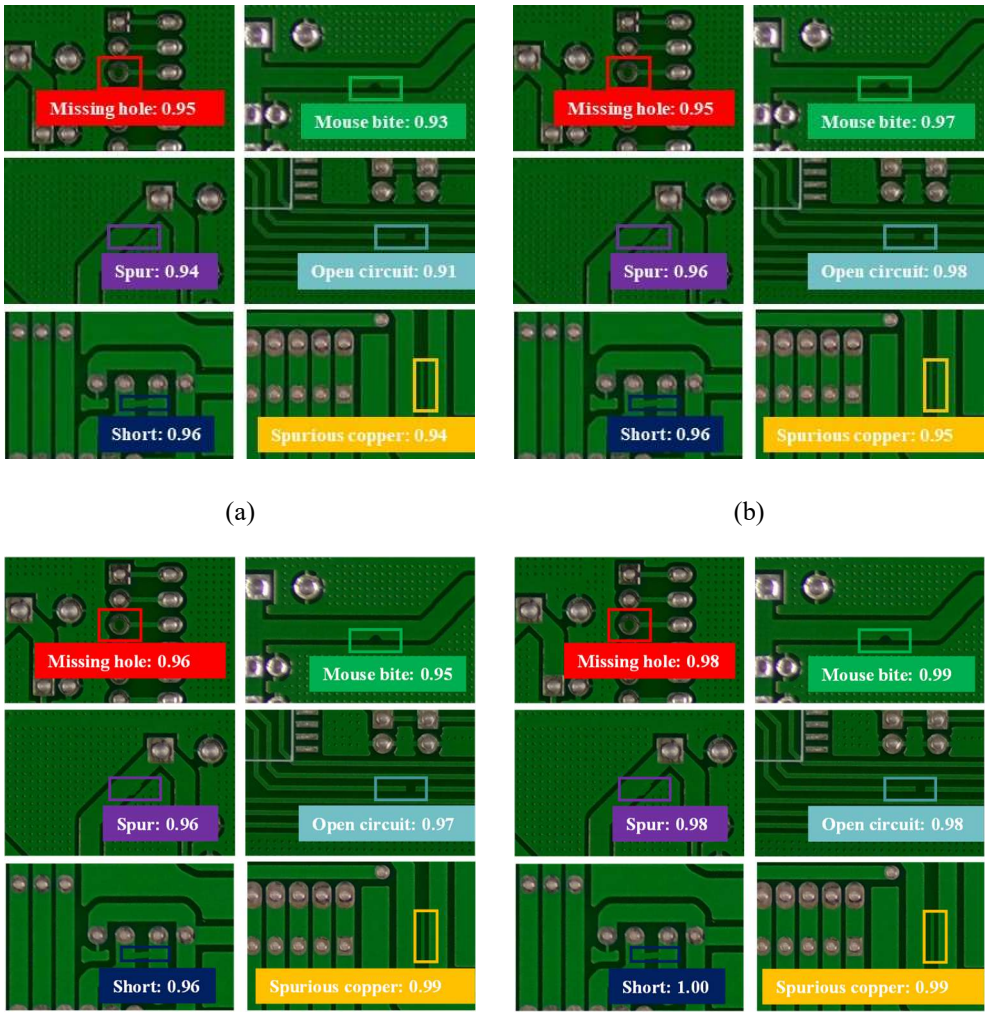

Figure 9: Comparison of the PCB defect detection results, (a) YOLOv8-nano, (b) YOLOv5, (c) YOLOv6, (d) Improved YOLOv8-CDSL.

The classification of surface defects on PCB is shown in Table 3. The improved YOLOv8-CDSL network has the highest *mAP* and maximum of 6 types of defects. The *mAP* is 99.13%. Compared to the YOLOv8-nano network, the *mAP* has improved by 4.52%. This shows that by adding C2f_DBB and SPFF_LSKA modules, the improved YOLOv8-CDSL network can effectively improve the accuracy of six types of PCB surface defects. The YOLOv5 and YOLOv6 networks demonstrate strong detection accuracy for PCB surface defects. The *mAP* of the improved YOLOV8-CDSL network is 3.67% and 1.47% higher than that of the YOLOv5 and YOLOv6 networks, respectively. These results indicate that the improved YOLOv8-CDSL network effectively detects PCB surface defects and achieves superior detection performance.

Table 3: Classification of surface defects on PCB.

Network	*mAP*(%)						*mAP*(%)
	Missing hole	Mouse bite	Spur	Open circuit	Short	Spurious copper	
YOLOv8-nano	95.12	94.97	96.17	94.09	95.14	93.59	94.85
YOLOv5	96.03	95.01	95.39	94.62	95.06	97.61	95.62
YOLOv6	98.47	96.53	97.46	97.91	97.35	98.47	97.70
Improved YOLOv8-CDSL (proposed)	99.69	99.27	98.91	98.24	99.67	99.02	99.13

IV. Conclusions

Aiming at the problem of high false detection rate of PCB defect detection,an improved YOLOv8-C2f_DBB-SPFF_LSKA (YOLOv8-CDSL) is used to detect defects of the PCB. The diverse branch block (DBB) is used to improve the faster version of CSP bottleneck with two convolutions (C2f) module in the YOLOv8 backbone network. The large separable kernel attention (LSKA) mechanism is also added to the SPPF module of the YOLOv8 network. The C2F_DBB module can significantly improve the model's ability to identify small-scale PCB defects, and greatly enhance the model's performance in comprehensive feature extraction. Thus significantly improving the overall accuracy of the model. The SPPF_LSKA module can reduce the computing power consumption of model training. Consequently, it significantly enhances the detection capability of the improved YOLOv8-CDSL network. The effectiveness of the improved scheme was verified by ablation experiments. At the same time, it is verified by comparative experiments that the improved YOLOv8-CDSL network has the highest detection accuracy of 99.13% for six common surface defects of PCB.

Data Sharing Agreement

The datasets used and/or analyzed during the current study are available from the corresponding author on reasonable request.

Competing Interests

The authors have no relevant financial or non-financial interests to disclose.

Acknowledgements

This work was supported by: 2022 Hubei Province High end Foreign Expert Project (No.2022EJD027), Innovation and Entrepreneurship Training Program Project of College Student, and Hubei Key Laboratory of intelligent transportation technology and device, Hubei Polytechnic University (2025XM102).

References

[1] Buga, C. S.; Viana, J. C. The role of printed electronics and related technologies in the development of smart connected products. Flex. Print. Electron. 2022, 7(4), 043001. http://doi.org/10.1088/2058-8585/ac91de.

[2] Zhou, Y.B.; Yuan, M.H.; Zhang, J.; Ding, G.F.; Qin, S.F. Review of vision-based defect detection research and its perspectives for printed circuit board. J. Manuf. Syst. 2023, 70, 557-578. https://doi.org/10.1016/j.jmsy.2023.08.019.

[3] Serban, M.; Vagapov, Y.; Chen, Z.; Holme, R.; Lipin, S. Universal platform for PCB functional testing. 2014 International Conference on Actual Problems of Electron Devices Engineering (APEDE) IEEE, Saratov, Russia, 25-26 September 2014; pp. 402-409. https://doi.org/10.1109/APEDE.2014.6958285.

[4] Sankar, V.U.; Lakshmi, G.; Sankar, Y.S. A review of various defects in PCB. J. Electron. Test. 2022, 38(5), 481-491. https://doi.org/10.1007/s10836-022-06026-7.

[5] Zhou, Y.B.; Yuan, M.H.; Zhang, J.; Ding, G.F.; Qin, S.F. Review of vision-based defect detection research and its perspectives for printed circuit board. J. Manuf. Syst. 2023, 70, 557-578. https://doi.org/10.1016/j.jmsy.2023.08.019.

[6] Zhang, K. Using deep learning to automatic inspection system of printed circuit board in manufacturing industry under the internet of things. Comput. Sci. Inf. Syst. 2023, 20(2), 723-741. https://doi.org/10.2298/CSIS220718020Z.

[7] Ulger, F.; Yuksel, S.E.; Yilmaz, A.; Gokcen, D. Solder joint inspection on printed circuit boards: a survey and a dataset. IEEE T. Instrum. Meas. 2023, 72, 1-21. https://doi.org/10.1109/TIM.2023.3277935.

[8] Ling, Q.; Isa, N.A.M. Printed circuit board defect detection methods based on image processing, machine learning and deep learning: a survey. IEEE Access. 2023, 11, 15921-15944. https://doi.org/10.1109/ACCESS.2023.3245093.

[9] Huang, B.; Liu, X.; Yan, J.W.; Xie, J.C.; Liu, K.; Xu, Y.; Liu, J.H.; Zhao, X.T. Fully automated dispensing system based on machine vision. Appl. Sci. 2023, 13(16), 9206. https://doi.org/10.3390/app13169206.

[10] Yu, X.Y.; Xiong, L.H.; Yang, H.D. Collaborative learning classification model for PCBs defect detection against image and label uncertainty. IEEE T. Instrum. Meas. 2023, 72, 1-8. https://doi.org/10.1109/TIM.2023.3235461.

[11] Wu, W.Y.; Wang, M.J.J.; Liu, C.M. Automated inspection of printed circuit boards through machine vision. Comput. Ind. 1996, 28(2), 103-111. https://doi.org/10.1016/0166-3615(95)00063-1.

[12] Liu, Z.C.; Qu, B.D. Machine vision based online detection of PCB defect. Microprocess. Microsy. 2021, 82, 103807. https://doi.org/10.1016/j.micpro.2020.103807.

[13] Li, J.; Gu, J.A.; Huang, Z.D.; Wen, J. Application research of improved YOLO V3 algorithm in PCB electronic component detection. Appl Sci. 2019, 9(18), 3750. https://doi.org/10.3390/app9183750.

[14] Chen, I.C.; Hwang, R.C.; Huang, H.C. Pcb defect detection based on deep learning algorithm. Processes. 2023, 11(3), 775. https://doi.org/10.3390/pr11030775.

[15] Zhang, C.; Shi, W.; Li, X.F.; Zhang, H.J.; Liu, H. Improved bare PCB defect detection approach based on deep feature learning. J. Eng. 2018, 2018(16), 1415-1420. https://doi.org/10.1049/joe.2018.8275.

[16] Ding, R.W.; Dai, L.H.; Li, G.P.; Liu, H. TDD-net: a tiny defect detection network for printed circuit boards. CAAI T. Intell. Techno. 2019, 4(2), 110-116. https://doi.org/10.1049/trit.2019.0019.

[17] Shen, J.Q.; Liu, N.Z.; Sun, H. Defect detection of printed circuit board based on lightweight deep convolution network. IET Image Process. 2020, 14(15), 3932-3940. https://doi.org/10.1049/iet-ipr.2020.0841.

[18] Mao, W.L.; Wang, C.C.; Chou, P.H.; Liu, Y.T. Automated defect detection in mass-produced electronic components via YOLO object detection models. IEEE Sens. J. 2024. https://doi.org/10.1109/JSEN.2024.3418618.
[19] Mamidi, J.S.S.V.; Sameer, S.; Bayana, J. A light weight version of PCB defect detection system using YOLOv4 tiny. 2022 International Mobile and Embedded Technology Conference, Noida, India, 10-11 March 2022; pp. 441-445. https://doi.org/10.1109/MECON53876.2022.9752361.
[20] Wang, J.; Li, Q.Q.; Fang, Z.Q.; Zhou, X.L.; Tang, Z.W.; Han, Y.L.; Ma, Z.L. YOLOv6-ESG: a lightweight seafood detection method. J. Mar. Sci. Eng. 2023, 11(8), 1623. https://doi.org/10.3390/jmse11081623.
[21] Li, S.S.; Guo, S.R.; Han, Z.L.; Kou, C.; Huang, B.C.; Luan, M.H. Aluminum surface defect detection method based on a lightweight YOLOv4 network. Sci. Rep-Uk. 2023, 13(1), 11077. https://doi.org/10.1038/s41598-023-38085-x.
[22] Ling, Q.; Isa, N.A.M.; Asaari, M.S.M. Precise detection for dense PCB components based on modified YOLOv8. IEEE Access. 2023, 11, 116545-116560. https://doi.org/10.1109/ACCESS.2023.3325885.
[23] Xia, K.W.; Lv, Z.L.; Liu, K.; Lu, Z.Y.; Zhou, C.D.; Zhu, H.; Chen, X.L. Global contextual attention augmented YOLO with ConvMixer prediction heads for PCB surface defect detection. Sci Rep-UK. 2023, 13(1), 9805. https://doi.org/10.1038/s41598-023-36854-2.
[24] Qiu, Z.F.; Wang, S.X.; Zeng, Z.X.; Yu, D.L. Automatic visual defects inspection of wind turbine blades via YOLO-based small object detection approach. J. Electron. Imaging. 2019, 28(4), 043023-043023. https://doi.org/10.1117/1.JEI.28.4.043023.
[25] Feng, B.X.; Cai, J.P. PCB defect detection via local detail and global dependency information. Sensors. 2023, 23(18), 7755. https://doi.org/10.3390/s23187755.
[26] Hou, Y.J.; Shi, G.; Zhao, Y.X.; Wang, F.; Jiang, X.; Zhuang, R.J.; Mei, Y.F.; Ma, X.J. R-YOLO: a YOLO-based method for arbitrary-oriented target detection in high-resolution remote sensing images. Sensors, 2022, 22(15), 5716. https://doi.org/10.3390/s22155716.
[27] Zhang, Q.Y.; Wang, C.; Li, H.; Shen, S.N.; Cao, W.; Li, X.Y.; Wang, D. Improved YOLOv8-CR network for detecting defects of the automotive MEMS pressure sensors. IEEE Sens. J. 2024. https://doi.org/10.1109/JSEN.2024.3419806.
[28] Guo, X.G.; Wang, N. Automated identification of pavement structural distress using state-of-the-art object detection models and nondestructive testing. J. Comput. Civil. Eng. 2024, 38(4), 04024014. https://doi.org/10.1061/JCCEE5.CPENG-5864.
[29] Nurmaini, S.; Rachmatullah, M.N.; Sanif, R.; Agustiansyah, P.; Sastradinata, I.; Legiran, L.; Darmawahyuni, A.; Sapitri, A.I.; Islami, A.; Firdaus, F.; Tutuko, B.; Lubis, N.M.E.R. Real time mobile AI-assisted cervicography interpretation system. Inform. Medicine Unlocked. 2023, 42, 101360. https://doi.org/10.1016/j.imu.2023.101360.
[30] Shen, L.Y.; Lang, B.H.; Song, Z.X. DS-YOLOv8-based object detection method for remote sensing images. IEEE Access. 2023, 11, 125122-125137. https://doi.org/10.1109/ACCESS.2023.3330844.
[31] Feng, B.X.; Cai, J.P. PCB defect detection via local detail and global dependency information. Sensors. 2023, 23(18), 7755. https://doi.org/10.3390/s23187755.
[32] Wang, Z.P.; Liu, D.; Wang, Z.W.; Liao, X.; Zhang, Q.L. A new remote sensing change detection data augmentation method based on mosaic simulation and haze image simulation. IEEE J. STARS. 2023, 16, 4579-4590. https://doi.org/10.1109/JSTARS.2023.3269784.
[33] Liu, Y.; Sun, P.; Wergeles, N.; Shang, Y. A survey and performance evaluation of deep learning methods for small object detection. Expert. Syst. Appl. 2021, 172, 114602. https://doi.org/10.1016/j.eswa.2021.114602.
[34] Song, Q.B.; Guo, Y.C.; Shepperd, M. A comprehensive investigation of the role of imbalanced learning for software defect prediction. IEEE T. Software. Eng. 2018, 45(12), 1253-1269. https://doi.org/10.1109/TSE.2018.2836442.
[35] Oksuz, K.; Cam, B.C.; Kalkan, S.; Akbas, E. One metric to measure them all: localisation recall precision (lrp) for evaluating visual detection tasks. IEEE T. Pattern Anal. 2021, 44(12), 9446-9463. https://doi.org/10.1109/TPAMI.2021.3130188.
[36] Sikati, J.; Nouaze, J.C. YOLO-NPK: a lightweight deep network for lettuce nutrient deficiency classification based on improved YOLOv8 Nano. Engineering Proceedings. 2023, 58(1), 31. https://doi.org/10.3390/ecsa-10-16256.
[37] Shi, Z.M.; Sang, M.; Huang, Y.K.; Xing, L.; Liu, T.G. Defect detection of MEMS based on data augmentation, WGAN-DIV-DC, and a YOLOv5 model. Sensors. 2022, 22(23), 9400. https://doi.org/10.3390/s22239400.
[38] Norkobil, S.S.; Abdusalomov, A.; Jamil, M.K.; Nasimov, R.; Kozhamzharova, D.; Cho, Y.I. A YOLOv6-based improved fire detection approach for smart city environments. Sensors. 2023, 23(6), 3161. https://doi.org/10.3390/s23063161.